

Numerical simulation of wind sand movement in straw checkerboard barriers

Ning Huang^a, Xianpan Xia, and Ding Tong

Key Laboratory of Ministry for Education on Western Disaster and Environment, Lanzhou University, Lanzhou 730000, China

Received 16 January 2013 and Received in final form 3 June 2013

Published online: 13 September 2013 – © EDP Sciences / Società Italiana di Fisica / Springer-Verlag 2013

Abstract. Straw checkerboard barrier (SCB) is the most representative antidesertification measure and plays a significant role in antidesertification projects. Large-eddy simulation and discrete-particle tracing were used to numerically simulate the wind sand movement inside the straw checkerboard barrier (SCB), study the movement characteristics of sand particles, find the transverse velocities of sand particles and flow field, and obtain the contour of the transverse velocity of coupled wind field within the SCB. The results showed that 1) compared with that at the inlet of the SCB, the sand transport rate inside the SCB greatly decreases and the speed of sand grain movement also evidently drops, indicating that the SCB has very good sand movement preventing and fixing function; 2) within the SCB there exists a series of unevenly distributed eddies of wind sand flow, their strength decreases gradually with increasing the transverse distance; 3) affected by eddies or reflux, sand particles carried by the wind sand flow have to drop forward and backward the two interior walls inside the SCB, respectively, forming a v-shaped sand trough; 4) the sand transport rate gradually decreases with increasing number of SCBs, which reveals that the capacity of the wind field to transport sand particles decreases. This research is of significance in sandstorm and land desertification control.

In recent years, wind-blown sand disasters represented by sandstorms and land desertification have become one of the most important environmental issues. In this respect, China has become one of the most affected countries in the world. The land subjected to desertification totals 1.74 million km², accounting for more than 18% of the total land area of China and affecting 30 of its province-level administrative regions [1,2]. From 2006 on, the area grows by 60 km² each year. Sandstorms caused by land desertification greatly harm ecological environment, transportation, communications, infrastructures, and social and economic development [3]. Facing severe sandstorm disasters, researchers have developed many antidesertification measures. The main techniques in the world to prevent desertification are shelterbelt, dune-building grass [4], sand fences [4–7], wind-break walls [8,9], cementing material, straw checkerboard barriers and so on. Among them, straw checkerboard barriers have great advantages over other techniques. They are cheaper, more convenient and more effective than other techniques [1]. The straw checkerboard barriers are successfully applied to the subgrade of Baotou-Lanzhou railway crossing the Tengger Desert of China as well as to other desert regions of China. This technique has now been introduced in developing countries like Ghana, Egypt

and Iran [1]. Therefore, the straw checkerboard barrier (SCB) technique plays a significant role in antidesertification projects.

SCB is an artificial sand-control measure to change the structures, direction, and intensity of the wind sand flow near the earth surface, and makes the surface of sands stable in the premise of not changing its chemical composition. It plays a double role to fix sand *in situ*, by stopping sand particles invasion and settling them down. SCB is installed mainly according to the motion patterns and the velocity of wind sand flow, the main direction of wind, the geomorphic characteristics, etc. Since the design of SCB and the layout of its spatial location are determined mostly based on practical experiences and repeated experiments, and people do not have sufficient knowledge of the laws of wind sand movement in the surrounding area of SCB, some antidesertification measures are often counterproductive. Instead of playing a role in antidesertification, they could become the hidden dangers of desertification. Some SCBs play a better role in sand control, but they are too expensive. Therefore, some researches put forward an optimal SCB design based on their theoretical analysis. For example, through the theoretical analysis of their model, Wang and Zheng [10] presented a row of ideally uniformly distributed eddies of sand within the SCB, based on which they calculated the optimal proportion of the height of the SCB above the grass to its

^a e-mail: huangn@lzu.edu.cn

side length using the analytic method of fluid mechanics. Ling *et al.* [11] proposed their model of an arc surface of sand, assuming that the chord tangent angle of the arc at the highest point is equal to the angle of repose of a dry sand dune, and obtained the approximate functional relationship between the side length of the SCB and the maximum depth of wind erosion in the SCB. Liu *et al.* [12] studied the principle of sand fixation and the efficiency of SCBs through their wind tunnel experiments. Some studies are consistent with the experimental results and some have been verified in practical projects and greatly advanced the researches on SCBs. However, in the actual cases, the flow field in the SCB is very complex, neither uniform nor steady; eddies in SCBs usually are not evenly distributed. Moreover, the flow field contains a series of complex factors as the two-phase flow, fluid-solid coupling, eddy generation and rupture, etc. Thus, it is difficult to find a concrete mathematical description of a so complex field of flow and impossible to obtain an accurate analytic solution. Furthermore, the dynamic characteristics of sand particles in the flow field in the SCB are also very complex. The shapes of sand dunes within the SCB continuously change with changing wind speed and direction. Limited by experimental conditions, the current wind tunnel experiments are difficult to accurately simulate the laws of motions of the flow field and sand particles in SCBs.

In this paper, the gas phase is described using the space-averaged hydrodynamic equation, and the turbulence stress is simulated with the large-eddy simulation method. The motion of sand particles is calculated with the discrete-element method, which was also used by Carneiro *et al.* [13] to study saltation of sand particles. Then the motion characteristics of the wind sand flow in the SCB and its surrounding areas are simulated by solving the model of wind sand motion with consideration of the coupling effects of wind field and sand particles [14], and the varying characteristics of the airflow passing the SCB and the motion characteristics of sand particles in the SCB are analyzed in detail.

1 Basic model and control equations

1.1 Fluid phase control equations

The control equations of turbulent flow motion of incompressible constant viscosity coefficient with particle motion are [15]

$$\frac{\partial}{\partial x_i}(V_f \rho u_i) = 0, \quad (1)$$

$$\frac{\partial(V_f u_i)}{\partial t} + \frac{\partial(V_f u_i u_j)}{\partial x_j} = -\frac{1}{\rho} \frac{\partial(V_f p)}{\partial x_i} + \frac{\partial(\nu \cdot 2S_{ij})}{\partial x_j} + F_i, \quad (2)$$

$$S_{ij} = \frac{1}{2} \left(\frac{\partial u_i}{\partial x_j} + \frac{\partial u_j}{\partial x_i} \right), \quad (3)$$

$$V_f = 1 - \sum_{i=1}^n (V_P / \Delta V), \quad (4)$$

where S_{ij} is the elongation tensor, ν the molecular viscosity coefficient, v_f the fluid volume fraction; ρ , μ , and p are the fluid density, velocity and pressure, respectively; F_i is the body force applied on the infinitesimal body, that is, the reaction force of the sand particles of each cell on flow field. According to the basic idea of large eddy simulation (LES), it is necessary to use an averaging method to distinguish the solvable large-scale eddy from the small-scale eddy to be modeled. Different from the Reynolds time-averaged method, LES uses the space-averaged method. In other words, the following formula can be used to transform the variable in eq. (1) into the large-scale solvable variable and subgrid modeling variable:

$$\overline{u_i}(x) = \int_{-\infty}^{+\infty} G(x-x') u_i(x') dx', \quad (5)$$

where $G(x-x')$ is a filter function. The filtered turbulence control equation is

$$\begin{aligned} \frac{\partial(V_f \overline{u_i})}{\partial t} + \frac{\partial(V_f \overline{u_i} \cdot \overline{u_i})}{\partial x_j} = \\ -\frac{1}{\rho} \frac{\partial(V_f \overline{p})}{\partial x_i} + \nu \frac{\partial(V_f 2\overline{S_{ij}})}{\partial x_j} - \frac{\partial \tau_{ij}}{\partial x_j}. \end{aligned} \quad (6)$$

The subgrid-scale stress is defined as $\tau_{ij} = \rho \overline{u_i u_j} - \rho \overline{u_i} \overline{u_j}$. In accordance with the Smagorinsky's SGS model, assuming that the SGS stress has the following form:

$$\tau_{ij} - \frac{1}{3} \delta_{ij} \tau_{kk} = -2\nu_t S_{ij}, \quad (7)$$

where ν_t is the turbulent viscosity of the subgrid scale:

$$\nu_t = (c_s \Delta)^2 \sqrt{2\overline{S_{ij} S_{ij}}}, \quad (8)$$

where the value of c_s is taken in the range 0.1–0.2 [16]. Its specific value is determined depending on specific circumstances given.

1.2 Equation of particle motion

If the forces applied to particles only are the gravity F_g and the drag force of fluid F_D , then

$$F_g = \frac{1}{6} \pi \rho_p D^3 g, \quad (9)$$

$$F_D = \frac{1}{8} C_D \pi D^2 \rho |V_r| V_r, \quad (10)$$

where ρ_p is the particle density, D the particle size, $C_D = (0.63 + 4.8/Re^{1/2})^2$ the fluid drag coefficient, $Re = V_f \rho D |V_r| / \mu$ the Reynolds number, $V_r = [(u-u_D)^2 + (w-w_D)^2]^{1/2}$ the relative velocity, u_D and w_D are the velocity components of the particle in the x - and z -direction, respectively. Thus, the sand particle motion equations is

$$m_p \frac{dU_D}{dt} = F_g + F_D, \quad (11)$$

where m_p and U_D are the mass and the velocity of sand particles, respectively.

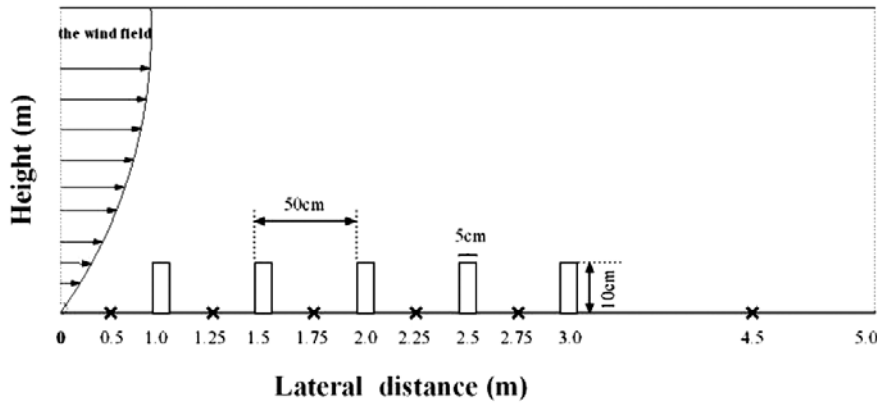


Fig. 1. Schematic of the computational area.

1.3 Processes of the sand and bed collision, and the sand and SCB surface collision

An airborne dust particle subject to the gravity acceleration falls toward and impacts the bed surface at a great velocity. At the same time when it rebounds, it will splash some particles with which it collides, which is the so-called splashing process and has been previously described using sputtering functions in wind tunnel experiments [17–21]. The three sputtering functions used in this paper are as follows.

1) Relationships of the rebounding velocity and angle to the incident angle and velocity of particles [22]:

$$|V_{re}| = 0.3|V_{im}| \pm 0.25|V_{im}|, \quad (12)$$

$$a_{re} = 30^\circ \pm 15^\circ. \quad (13)$$

2) Relationship of the velocity and angle of the splashed particles to the incident particles:

$$|V_{ej}| = 0.3|V_{im}| \pm 0.5|V_{ej}|, \quad (14)$$

$$a_{ej} = 55^\circ \pm 5^\circ. \quad (15)$$

3) Relationship of the number of splashed particles to the angle and velocity of incident particles [23]:

$$N_p = \max[0, 3.36 \sin(\alpha_{im})(5.72V_{im} - 0.915)]. \quad (16)$$

Because the collision process between sand particles and SCB is very complex and has not been studied in depth, for a flexible body model we have the following assumption:

$$V_{re} = (0.4, 0.5)V_{im}, \quad (17)$$

where (0.4, 0.5) means that the value is taken in between the range (0.4, 0.5) according to the average probability density function.

1.4 Calculation model and boundary conditions

According to Wang *et al.* [10], let the height of the SCB above the grass and the sand barrier distance be 10 cm

and 50 cm, respectively. Figure 1 shows the schematic diagram of our calculated area and model. The height and width of the barriers are 10 cm and 5 cm, respectively. The interval between barriers is 50 cm. L is the lateral distance from inlet in the X -direction and the positions of $L = 0$ m and $L = 5$ m represent the inlet and outlet of the computational area, respectively. In this paper, the sand transport rates and the transverse speeds of sand particles at $L = 0.5$ m, 1.25 m, 1.75 m, 2.25 m, 2.75 m, and 4.5 m are analyzed in sect. 2.

The logarithmic profile line is taken for the initial velocity of the wind field at the inlet and the axial wind speed is taken as 10 m/s in the calculation, thus by using

$$u = \frac{u_*}{k} \ln \frac{z}{z_0}, \quad (18)$$

the corresponding friction wind speed is found to be 0.34 m/s. In eq. (18), $z_0 = D_p/30$ is the bed surface roughness, D_p the size of sand particles. To facilitate the comparison between the calculated results of the wind sand flow and the experimental results of the wind tunnel, the size of sand particles is chosen as 0.295 mm based on the average particle diameter in the wind tunnel experiment.

The upper boundary is the open boundary condition, when the wind field is fully developed and the upper boundary is high enough so that the wind flow is not disturbed by the surface, the wind field has no velocity gradient in the X -direction. That is, the derivative of horizontal position is equal to zero: $\frac{\partial u}{\partial x} = 0$ [15].

The lower boundary is the nonslip boundary condition: $u = v = 0$.

The equation is made discrete by using the finite volume method. The calculation area is 5 m long \times 1 m high, and divided into 500 \times 100 grids. The grid in the height direction is refined layer-by-layer by using logarithmic law. The steady state saltation wind sand flow on the flat surface in the same inlet wind velocity condition was first generated after comparing with the results of the wind tunnel experiment, and used as the initial condition for particle calculation. The time steps for the fluid control equation and the particle motion equation are taken as

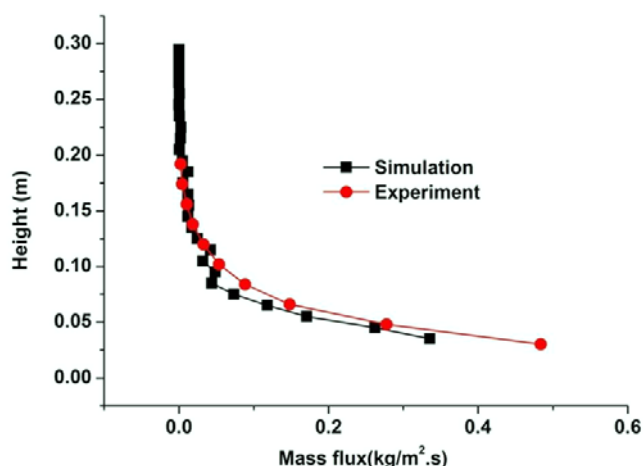


Fig. 2. Comparison between the calculated results and wind tunnel experimental results on changes in sand transport rate over height.

0.01 s and 0.0001 s, respectively, and the total calculation time is 25 s.

2 Calculation results and discussion

According to the selected length of the computational domain, the wind speed, sand transport rate and particle movement speed at six points in the x -axis, 0.5 m, 1.25 m, 1.75 m, 2.25 m, 2.75 m and 4.5 m, were chosen as numerical data in our analytic approach.

2.1 Changes in sand transport rate

In the numerical simulation, the incoming wind field at the inlet used is the smooth flow. The calculated sand transport rate of the steady saltation wind sand flow at the inlet was compared with the result of experiments with the wind sand flow at the same wind speed on the smooth sand bed surface in the multifunctional environment wind tunnel of Lanzhou University, Gansu Province, China. Figure 2 shows numerically simulated results of the sand transport rate over the height at the inlet and the results of the wind tunnel experiment. From the figure it is obvious that the two results are in a good agreement, thus confirming that our calculation is accurate.

Figure 3 shows the relationship of the sand transport rate to height at different distances from the inlet. It clearly shows that compared to that at the distance $L = 0.5$ m, the sand transport rates within the SCB are very small. It also can be seen from the inset graphic that the sand transport rate within the SCB always shows a trend first to increase and then to decrease with height. Compared to that of the first SCB, the sand transport rates of the latter ones are smaller and smaller. The results indicate that most sand particles movements within SCBs will be stopped or blocked by the barriers, and only very few could pass over them, which further confirm that

the SCB has good sand movement prevention and fixation effects.

The ratios of mass flux of the particles at the outlet to that at the inlet could measure the efficiency of the SCB. In this paper, the ratios of the mass flux at $L = 1.25$ m, 1.75 m, 2.25 m, 2.75 m and $L = 4.5$ m to the mass flux of inlet are 9.831%, 7.207%, 4.713%, 1.922% and 1.404%. The percentage of the particles that can pass over all the SCBs is 1.404% and the efficiency of the SCBs is 98.596%. It is thus clear that the sand fixation efficiency of the SCB is very high.

2.2 Changes in velocities of flow field and particle motion

Figure 4 is a simulated contour map of the transverse velocity of the coupled wind field and the streamline diagram within the SCB. It clearly shows that a series of eddies exist within the SCB and their strength becomes smaller with increasing the lateral distance. In other words, eddies are unevenly distributed within the SCB. Due to the presence of the reflux zone, the refluxing characteristic occurs when the sand particles falling in the SCB accumulate and reach a certain amount. When sand particles are blocked by the SCB, fall to the back side within the SCB, and pile up, a fair part of “dead” particles flow in the inverse direction of the wind field and pile up in the front side of the SCB, only relatively fewer sand grains are kept in its center, forming at last a smooth sand pit within the SCB at its bottom. This is a typical phenomenon in the presence of eddies, which is also well reflected in the results of our numerical simulation.

Figure 5 shows a sequence of snapshots about the evolution of the particle distribution over time. To explain fig. 5, we first give some definitions. The dead particles are the particles which deposit in the surface when they move into SCBs. The rebounding particles are particles which rebound in to air when they impact the bed or the SCB. The particles passing over the SCB means these particles do not fall down into the SCBs when they move across the SCBs. From fig. 5, we can observe the movement and distribution of sand particles in the SCB. After the incoming wind sand flow has hit the SCB, a part of them falls to it and piles up to form “dead” particles, another part of them rebounds, accelerates forward in the action of wind, drops into another SCB and splashes some sand particles at the same time. Most of the particles squashed will be blocked and stay in this SCB, only a very small part of them will pass over all the SCBs into the no-SCB zone.

Figure 6 shows the velocity distribution of sand particles within the SCB. Compared with the particle motion at the inlet, there are evident variations in the velocities at which the sand particles move within the SCB. From fig. 6, it is clear that except the no-SCB point at $L = 0.5$ m, the particles’ velocities at other points have the sections of smaller-than-zero velocities, or negative velocities. In other words, there is a reflux zone in the SCB where the sand particles will move in the reverse direction. The transverse velocities of particles’ movement inside the

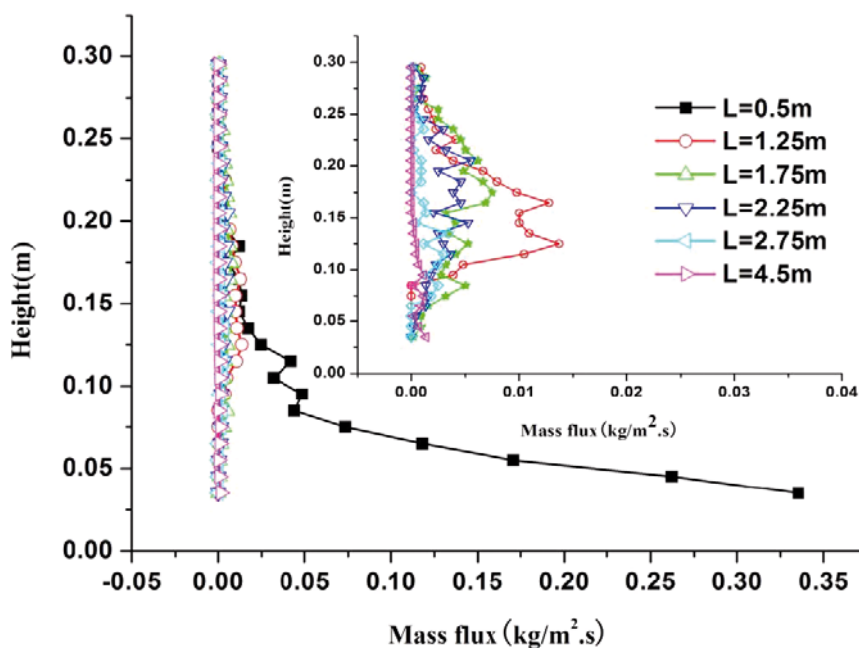


Fig. 3. Relationship of sand transport rate to height along the path with distance from the inlet (L as a parameter).

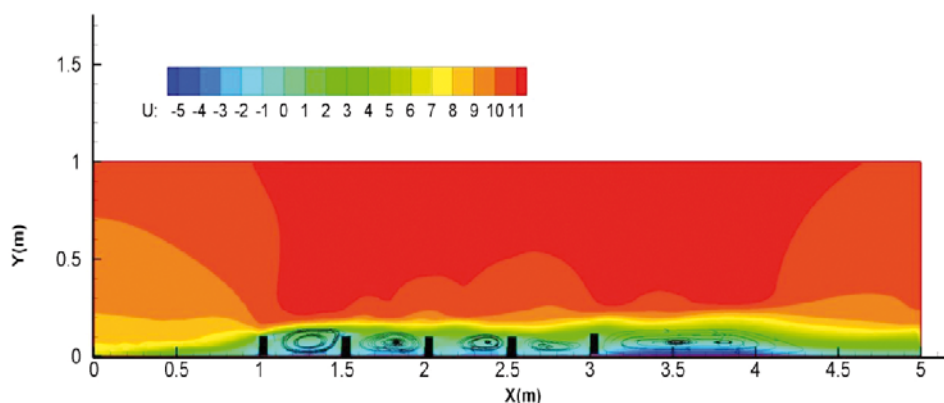


Fig. 4. Contour of the transverse velocity of coupled wind fields.

SCB are mostly smaller than their velocities at the inlet; while at the upper part inside the SCB the particles' velocities increase with the height and are even higher than those at the inlet, which reveals that the presence of SCBs accelerates the velocities of sand particles at the top and makes the particles there obtain more energy from the wind field.

3 Conclusions

In this paper, we used large-eddy simulation and discrete-particle tracing to numerically simulate the wind sand movement inside the SCB, studied the movement characteristics of sand particles, and calculated the transverse velocities of sand particles and flow field and obtained the contour map of the transverse velocity of the coupled wind field within the SCB. The results showed that 1) compared

with that at the inlet of the SCB, the sand transport rate inside the SCB greatly decreases, the speed of sand grain movement also evidently drops, indicating that the SCB has very good sand movement preventing and fixing function; 2) within the SCB, there exists a series of unevenly distributed eddies of wind sand flow; their strengths decrease gradually with increasing the transverse distance; 3) affected by eddies or reflux, sand particles carried by the wind sand flow have to drop forward and backward the two interior walls inside the sand barrier, respectively, forming a v-shaped sand trough; 4) the sand transport rate gradually decreases with increasing the number of SCBs, which reveals that the capacity of the wind field to transport sand particles decreases. Moreover, we also numerically simulated the spatial distribution and motion vector of sand particles to visually show their movement and distribution in the SCB and dynamically display the entire process of blocking and fixing sand particles. The

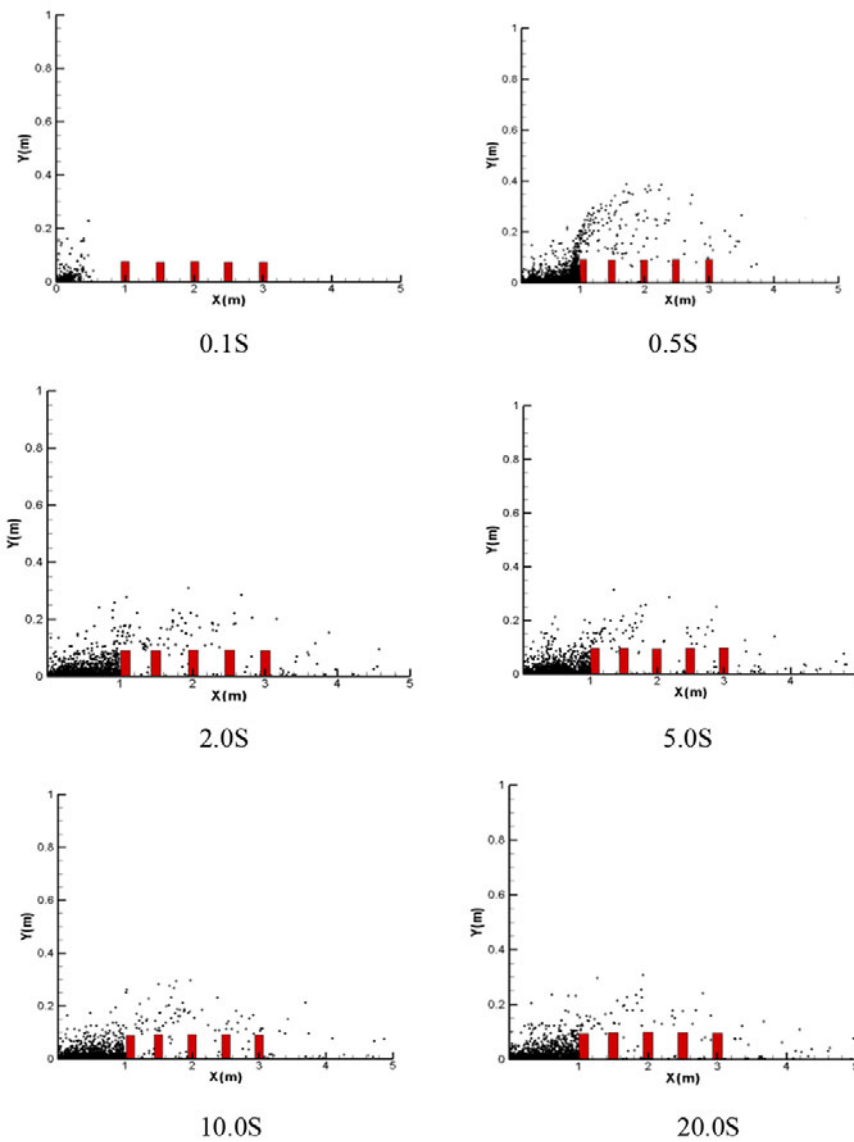


Fig. 5. Spatial distribution of sand particles.

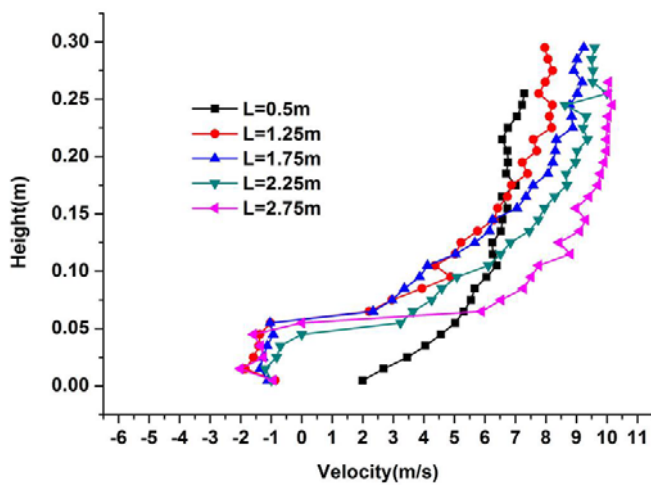


Fig. 6. Relationship of transverse speed to height along the path with distance from the inlet (L as a parameter).

numerical results show that the SCB do have good effects on sand fixation and it is possible to widely extend the SCB usage in sand fixation projects. These simulated results are useful to understand the sand fixation mechanism of the SCB and may be helpful to model dunes to consider the influence of the SCB on the evolution of dune fields [24–26]. To get more precise results, the next study will concentrate on the collision process between sand particles and the SCB by wind tunnel experiments and theoretical analysis so that the splash function between sand particles and SCBs, which is a simple assumption in this paper will be improved.

This work is supported by the National Key Basic Research and Development Program (“973” Program) (2009CB421304), the Innovative Research Groups of the National Natural Science Foundation of China (11121202) and the National Natural Science Foundation of China (11172118, 40971009).

References

1. X.J. Zheng, *Mechanics of Wind-blown Sand Movement* (Springer, 2009).
2. T. Wang, G.T. Wang, Z.G. Qian, G.S. Yang, J.J. Qu, D.L. Li, *Chin. J. Desert Res.* **21**, 322 (2001).
3. X.J. Zheng, Y.H. Zhou, *Mech. Engin.* **25**, 11 (2003).
4. Kenneth Pye, Haim Tsoar, *Aeolian Sand and Sand Dunes* (Springer, 2009).
5. Katsumori Hatanaka, Shiataro Hotta, *Int. J. Numer. Methods Fluids* **24**, 1291 (1997).
6. John D. Wilson, *J. Appl. Meteorol.* **43**, 1392 (2004).
7. J.P. Bitog, I.B. Lee, M.H. Shin, *et al.*, *Atmos. Environ.* **43**, 4612 (2009).
8. T. Bouvet, J.D. Wilson, A. Tuzet, *J. Appl. Meteorol. Climatol.* **45**, 1332 (2006).
9. J.L. Santiago, F. Martin, A. Cuerva, *et al.*, *Atmos. Environ.* **41**, 6406 (2007).
10. Z.T. Wang, X.J. Zheng, *Chin. J. Desert Res.* **22**, (2002).
11. Z.D. Zhu, Z.L. Zhao, Y.Q. Lin, *Desert Control Engineering* (Environmental Science Press, Beijing, 1998).
12. X.W. Liu, *Wind tunnel experiments of Straw checkerboard barriers* (Ningxia People's Publishing House, Yinchuan, 1988).
13. M.V. Carneiro, T. Pätz, H.J. Herrmann, *Phys. Rev. Lett.* **107**, 098001 (2011).
14. B.S. Anderson, P.K. Haff, *Wind modification and bed response during saltation of sand in air* (Springer-Verlag, 1991).
15. Y.P. Shao, A. Li, *Boundary-Layer Meteorol.* **91**, 199 (1999).
16. D.J. Tritton, *Physical Fluid Dynamics* (van Nostrand Reinhold Company, 1977) pp. 21-23.
17. B.R. White, J.C. Schulz, *J. Fluid Mech.* **81**, 497 (1977).
18. B.B. Willetts, M.A. Rice, *Acta Mechan.* **63**, 255 (1986).
19. B.B. Willetts, I.K. McEwan, M.A. Rice, *Acta Mechan.* (suppl.1) , 23 (1991).
20. I.K. McEwan, B.B. Willetts, *J. Fluid Mech.* **52**, 99 (1993).
21. S. Mitha, M.Q. Tran, B.T. Werner, P.K. Haff, *Acta Mech.* **63**, 267 (1986).
22. I. Vinkovic, C. Aguirre, M. Ayrault, S. Simoëns, *Boundary-Layer Meteorol.* **121**, 283 (2006).
23. B.T. Werner, *J. Geol.* **98**, 1 (1990).
24. Marco C. M. de M. Luna M, Eric J. R. Parteli, Orenco Durán, *et al.*, *Geomorphology* **129**, 215 (2011).
25. Marco C. M. de M. Luna M, Eric J. R. Parteli, Hans J. Herrmann, *Geomorphology* **159-160**, 169 (2012).
26. T.L. Bo, X.J. Zheng, *Geomorphology* **180-181**, 24 (2013).